Preparation and characterization of TiO_2 photocatalysts co-doped with Iron (III) and lanthanum for the degradation of organic pollutants

QIANGQIANG WANG, SHIHUA XU, FENGLEI SHEN*
College of Chemistry, Chemical Engineering and Materials Science, Soochow University, Suzhou 215123, China

Titanium dioxide photocatalysts co-doped with Iron (III) and lanthanum were prepared by a facile sol–gel method. The structure of catalysts was characterized by X-ray diffraction (XRD), Raman spectroscopy, UV–vis diffuse reflectance spectroscopy and X-ray photoelectron spectroscopy (XPS). The photocatalytic activities of the samples were evaluated by the degradation of methylene blue in aqueous solutions under visible light (λ>420 nm) and UV light irradiation. The probable mechanism of co-doped particles was investigated by analyzing the structures and photocatalytic activities of the undoped, Iron and/or lanthanum singly doped and co-doped TiO_2. The results of XRD, Raman and XPS indicate that Fe^{3+} ions substituted for Ti^{4+} in the lattice of TiO_2 and lanthanum ions existed within the crystal matrix or on the surface of TiO_2 as the form of La_2O_3 particles. In addition, diffuse reflectance measurements show an extension of light absorption into the visible region by these dopants. Compared with Fe^{3+} or La^{3+} singly doped TiO_2, the codoped TiO_2 exhibits excellent visible light and UV light activity and the synergistic effect of Fe^{3+} and La^{3+} is responsible for improvement of the photocatalytic activity.

(Received January 13, 2011; accepted February 17, 2011)

Keywords: Titania, Fe^{3+} doped, La^{3+} doped, Co-doped, Photocatalysts, Synergistic effect

1. Introduction

Photocatalytic degradation of organic pollutants on semiconductor surfaces offers a viable approach to the solution of a variety of environmental problems. Semiconductor TiO_2 is the most widely used material because of its advantages such as high oxidation rate, low material cost, non-toxicity, chemically stability, and ecological friendliness [1-4]. However, a major drawback of pure TiO_2 anatase phase is that the bandgap (Eg) is about 3.2 eV, which requires excitation wavelengths of λ< 376 nm. Therefore, only 5–8% of sunlight photons have the enough energy to activate the catalyst. In addition, the high recombination rate of photoinduced electron-hole pairs results in poor efficiency of photocatalytic reactions. In that case, the overall efficiency of pure TiO_2 is quite low, and the practical application is limited [5-9]. To deal with these problems, several strategies have been involved such as depositing noble metals on TiO_2 surface and doping with foreign species [10]. Among them, doping could be the effective way to improve the photocatalytic activity of TiO_2 under the visible light irradiation [5].

Transition metal dopants have been widely used to improve the photoefficiency of the electronic process as well as the response to the visible part of the spectrum. Iron is frequently employed owing to its unique half-filled electronic configuration, which might narrow the energy gap though the formation of new impurity energy levels [11, 12]. Choi et al. [13] evaluated the effect of 21 different kinds of metal ions doping on the photoreactivity of TiO_2. Fe^{3+} dopant showed to be better than other metal ions. The most accepted explanation for improved photocatalytic performance of Fe^{3+}-doped samples is that Fe^{3+} dopant can form shallow charge traps within the TiO_2 crystal lattice through the substitution of Ti^{4+}, which reduced the electron–hole recombination and improved the photocatalytic efficiency [14-16].

Transition metal-doped TiO_2 photocatalysts are active under visible-light irradiation; however, the efficiency is insufficient for practical use due to low thermal instability [1]. Recently, doping rare earth metals such as La, Eu and Ce has received much attention [17-19]. In the published work, the report proved that TiO_2 with rare earth metal dopants shows significant improvement on both the photocatalytic activity and the thermal stability usually [20-22].

Doping with transition metal or rare earth metal elements has its respective advantage. The previous research showed two dopants had more synergistic effect than a single one for enhancing the absorption in the visible-light region and improving the photocatalytic activity of TiO_2 [23, 24]. The sample may possess the better photocatalytic performance if transition metal and rare earth metal elements are codoped into TiO_2. To the best of our knowledge, few reports dealt with TiO_2 photocatalyst codoped with Fe^{3+} and La^{3+} for photo-oxidative degradation of organic pollutants. Here, we prepared TiO_2 photocatalysts codoped with Fe^{3+} and

La^{3+} by a facile sol–gel method and its photocatalytic activities have been tasted for degradation of organic compound under both UV light and visible light irradiation. As expected, TiO_2 photocatalysts co-doped with Iron (III) and lanthanum with excellent visible light and UV light activity have been demonstrated and $Fe^{3+}$and La^{3+} have synergistic effects on improving the photocatalytic activity under both visible and UV light irradiation.

2. Experimental

2.1 Materials and synthesis

All the chemicals used in the experiments were reagent grade and used as received without further purification. Tetrabutyl titanate, ferric nitrate and lanthanum nitrate were used as starting materials. The material was prepared via a facile sol-gel route as follows. First, 10 mL Tetrabutyl titanate was mixed with 40 mL anhydrous ethanol (solution A). Solution B consisted of 1.0 mL deionized water, 10 mL anhydrous ethanol and 1 mL 70% HNO_3, ferric nitrate and lanthanum nitrate in the required stoichiometry (Fe: La: Ti = 0.002: 0.02: 1, molar ratio). Then solution A was added dropwise into solution B under vigorous stirring at room temperature for 12h until the transparent sol was obtained. After being dried in air at 80 ^oC for 12 h, the obtained mixture was calcined at various temperature from 300 to 800 ℃. The sample was designated as Fe-La-TiO_2. Fe^{3+}, La^{3+} single doped TiO_2, and pure TiO_2 were prepared following the same procedure. They were designated as Fe-TiO_2, La-TiO_2 and pure TiO_2, respectively.

2.2 Catalyst characterization

X-ray diffraction (XRD) patterns were obtained with a Rigaku D/Max diffractometer operating at 40 kV, 30 mA with Bragg–Brentano geometry using Cu Kα radiation (λ=1.5405 Å). The scan ranged from 20°to 80° (2θ degree) with a scan rate of 3° min^{-1}. The S_{BET} of the samples were determined through nitrogen physical adsorption at 77 K (Micromeritics ASAP 2010). All the samples were degassed at 150 ^oC before the measurement. Raman measurements were performed at room temperature using a Via+ Reflex Raman spectrometer with the excitation light of 514 nm. X-ray photoelectron spectroscopy (XPS) were performed on a SPECS ESCA system with Mg Kα source (hν = 1253.6 eV) at 10.0 kV and 20.0 mA. The UV–visible diffuse reflectance spectra were obtained using a scan UV–vis spectrophotometer (Varian Cary 500) equipped with an integrating sphere assembly, while $BaSO_4$ was used as the reference material and the analysis range was from 200 to 800 nm.

2.3 Photocatalytic activity

The photocatalytic activity of each simple was evaluated by the degradation of methylene blue (MB) in TiO_2 aqueous solution under UV and visible light irradiation. A 300-W high-pressure Hg lamp for which the predominated irradiation wavelength is 365 nm was used as a UV light source. A 1000-w halogen lamp equipped with a UV cut-off filters ($\lambda > 420$ nm) was used as a visible light source. The photocatalyst (0.10g) was added into an 100-mL quartz photoreactor containing 80 mL of a 1.0×10^{-4} g L^{-1} MB solution which. The photoreactor was cooled with flowing water in a quartz cylindrical jacket around the reactor, and ambient temperature was maintained at 25 ^oC during the photocatalytic reaction. The suspension was stirred in dark for 30 min to in order to reach the adsorption–desorption equilibrium. Then the suspension was irradiated under UV and visible-light. Samples were withdrawn periodically from the reactor, then centrifuged and analyzed by recording variations in the absorption in the UV–vis spectra of RB using a Cary 500 UV–vis spectrophotometer at its characteristic wavelength (λ=665 nm).

3. Results and discussion

3.1 X-ray diffraction

XRD measurements were performed to identify the crystalline phases synthesized by the sol-gel process at calcination temperatures ranging from 300 to 800 °C. Fig. 1 exhibits XRD patterns of pure TiO_2, Fe-TiO_2, La-TiO_2 and Fe-La-TiO_2 calcinated at 500 and 800 ^oC. It can be seen that the diffraction peaks of all samples which calcinated at 500 ℃ are ascribed to the peaks of TiO_2 anatase phase. When the calcination temperatures increased to 800 ^oC, rutile phase appears in sample of pure TiO_2 and Fe-TiO_2, while anatase is still the unique phase in sample of La-TiO_2 and predominant phase in the sample of Fe-La-TiO_2. No obvious diffraction peaks that could be attributed to the dopants are observed. Thus, the crystal structure of TiO_2 indicates a mixture of anatase and rutile for all samples. These results suggest that the doping levels that were employed or the subsequent thermal treatments did not induce the formation of discrete impurity phases. However, it is conceivable that dopants, which were formed during prepares, were nanoscopic or possibly dispersed on the surface [25]. It could be assumed that Fe^{3+} ions are most likely substituted in Ti^{4+} sites within TiO_2 because the ionic radius of Fe^{3+} ion (0.64 Å) is similar to Ti^{4+} ion (0.68 Å). In contrast, La^{3+} ions are most likely to be found as dispersed metal oxides within the crystal matrix or on the surface of TiO_2 because of the relatively large size difference between La^{3+} (1.15 Å) and Ti^{4+}.

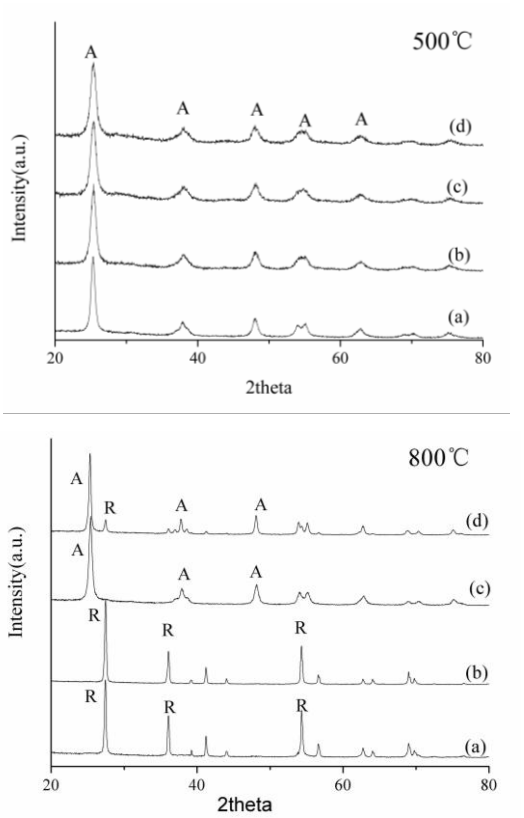

Fig. 1. XRD patterns measured for (a) pure TiO_2, (b) Fe-TiO_2, (c) La-TiO_2 and (d) Fe-La-TiO_2 with different calcination temperature (at 500 and 800 ^oC).

The anatase-to-rutile (A-R) phase transformation of pure TiO_2 normally occurs between 600-700 °C [26]. It could be seen that the rutile phase appears for pure TiO_2 and Fe-TiO_2 when calcining temperature is 800 ^oC, while anatase phase is still unique phase for La-TiO_2 and predominant phase for Fe-La-TiO_2 samples when the calcining temperature is 800℃. These demonstrated that Fe^{3+} dopants lower the A-R phase temperature of TiO_2 while La^{3+} dopants higher the temperature. Zhang et al. [27] reported that Fe^{3+} dopants decrease of the phase transition temperature at high Fe^{3+} concentrations (5at. %). They had been attributed it to surface effects. We have been observed the same phenomenon at low Fe^{3+} concentrations (0.2 at. %). Jina choi et al. [25] reported that La^{3+} dopant have little impact on the A-R phase transformation at low La^{3+} concentrations (0.3 at. %). However, we have been observed that La^{3+} dopant could inhibit the A-R phase transportation at high La^{3+} concentrations (2at. %). Therefore, we could concluded that the doping effect of metal ions on the A-R phase transformation is dependent on the intrinsic physicochemical properties of the doping metal ion but also the specific concentration of the individual dopants.

The average crystallite size of the samples was estimated by the Scherrer equation and the values were given in Table 1. As can be seen from the values, the crystallite size of Fe-doped TiO_2 is larger than the undoped TiO_2, which indicates that Fe-doping provide improvement on the crystallization degree of the rutile phase. However, some previous studies reported controversial results of Fe^{3+} doping effect on the crystallite sizes. For example, Yang et al. [11] reported that Fe^{3+} decrease the crystallite sizes. Referring to the phase composition of the sample, we presume that the dominant rutile phase might lead to the particle size increasing, whereas the anatase phase is just the opposite in the Fe^{3+} dopants samples. With addition of La^{3+}, the crystallite size of samples was significantly decreased.

Table 1. Property of catalysts.

Calcination Temperature (^oC)	Catalyst	Surface Area($m^2\ g^{-1}$)	Average Size(nm)
500	pure TiO_2	63	14
	Fe-TiO_2	78	12
	La-TiO_2	75	11
	Fe-La-TiO_2	84	10
800	Pure TiO_2	29	28
	Fe-TiO_2	25	30
	La-TiO_2	39	25
	Fe-La-TiO_2	46	22

3.2 BET surface areas

As is shown from Table 1, all dopants simples have larger surface areas than pure TiO_2, which calcined at 500 ^oC. When the calcination temperatures increased to 800 ^oC, Fe-TiO_2 has the minimum surface areas due to an increase in the particle size in rutile phase. The large surface areas may attribute to the high photocatalytic activities of the samples.

3.3 Raman studies

Raman spectra of the samples which were calcined at 500 ^oC are shown in Fig. 2. Rutile single crystals have Raman peaks at 142 cm^{-1} (B_{1g}), 234 cm^{-1} (Eg), 445 cm^{-1} (Eg), and 608 cm^{-1}(A_{1g}) [22]. All these peaks were clearly visible in the spectra of pure TiO_2 and Fe-TiO_2, indicating that rutile crystal is the predominant species. No Raman lines corresponding to iron oxide can be observed in the Fe^{3+} doped samples, confirming Fe^{3+} may present in the substitutional positions in the lattice of TiO_2. The Raman spectra of La-TiO_2 and Fe-La-TiO_2 are characterized at 144 cm^{-1}(E_g), 395 cm^{-1}(B_{1g}), 514 cm^{-1}(A_{1g}) and 638 cm^{-1}(E_g), indicating that anatase nanoparticles are the predominant species [16]. The evolution of two additional Raman peaks at 445 cm^{-1} and 608 cm^{-1} is observed in the spectra of Fe-La-TiO_2 indicating that there is still rutile phase in the sample. The results are consistent with the XRD measurements.

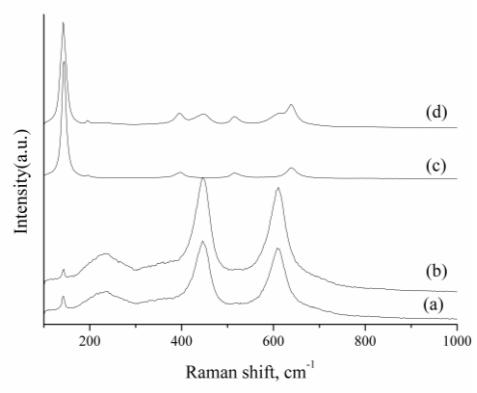

Fig. 2. Raman spectra of (a) pure TiO_2, (b) Fe-TiO_2, (C) La-TiO_2 and (d) Fe-La-TiO_2, which were calcined at 500 ^oC. Raman spectra for the samples calcined at 800 ^oC, which are not shown here, are identical with that of La-TiO_2 in the figure.

3.4 X-ray photoelectron spectroscopy

To investigate the chemical states of dopants in TiO_2, Ti2p, O1s, Fe 2p and La 3d core levels were measured by XPS. Ti2p, O1s, Fe 2p and La 3d XPS spectra of Fe-La-TiO_2 are shown in Fig. 3. With respect to the XPS peaks of Ti 2p, although there are slight differences in the locations of binding energies of Ti 2p1/2 and Ti 2p3/2 among different samples, they are all still in good agreement with the values of Ti^{4+}. No broad FWHM (full width at half maximum) of Ti 2p3/2 peak signals also indicates the only presence of Ti^{4+} species [28]. Comparing to the ones in the pure TiO_2, the small binding energy shifted to higher energies that may be attributed to the formation of the Ti–O–Fe bonds in the crystal lattice. The O 1s binding energies of all the samples are located at a little higher value than 529.7 eV corresponding to the value of the one in the pure TiO_2, which is assigned to bulk oxide (O^{2-}) in the TiO_2 lattice. The signals of Fe were found to be weaker than all the others, due to the low doping level. The binding energies around 710 eV are assigned to Fe 2p3/2 of Fe^{3+} [29]. The results indicate that Fe^{3+} penetrated into the TiO_2 lattice and substituted Ti^{4+} [30]. Since the radius of Fe^{3+} and Ti^{4+} is similar, the Fe^{3+} could be incorporated into the lattice of TiO_2 to form Ti–O–Fe bonds in Fe-TiO_2 and Fe-La-TiO_2 [31]. Regarding the La 3d core level spectra, we observe that a splitting of the La 3d 5/2 and the La 3d 3/2 at around of 835ev and 852ev in La-TiO_2 and Fe-La-TiO_2. Asha et al. [32] reported that lanthanum oxide (La_2O_3) films have a split of the La 3d XPS spectra giving two maxima. Ruiz et al. [33] reported that the 3d lines of La^{3+} have satellites. The interpretation of this splitting in the oxide was now widely accepted to be due to configuration effects in the final state of La. Therefore, the La XPS profiles observed in our samples are most probably as a form of lanthanum oxides.

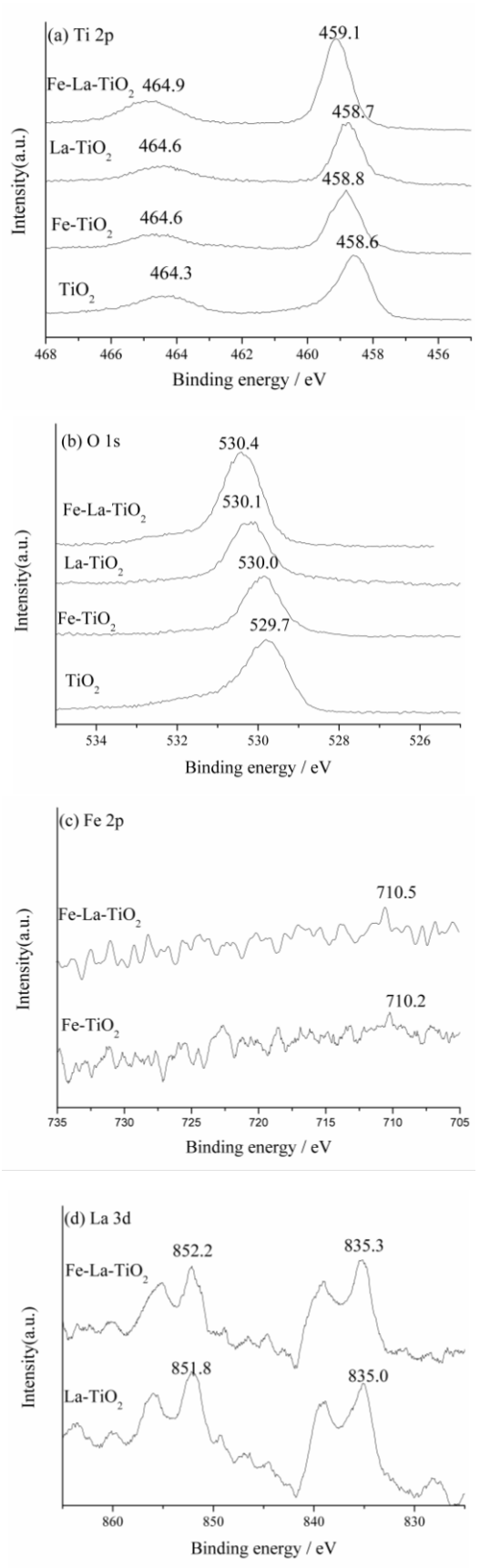

Fig. 3. XPS spectra of various samples: (a) Ti 2p, (b) O 1s, (c) Fe 2p, (d) La 3d.

3.5 UV–vis diffuse reflectance spectra

The UV–vis diffuse reflectance spectra of samples which were calcined at 500 °C are shown in Fig. 4. The pure TiO_2 are characterized by sharp absorption edges at about 400 nm. The spectrum of Fe-TiO_2 shows a significant enhancement of light absorption at a wavelength of 400-700 nm compared with pure TiO_2. The origin of this visible light absorption was due to the formation of impurity levels within the band gap of TiO_2. The electronic transitions between these impurity levels and the valence or conduction band effectively shift the band edge absorption to visible light region [16]. It may also originate from defects associated with oxygen vacancies that give rise to colored centers. Although the curve shape of the spectrum of TiO_2 nanoparticles do not nearly change after La^{3+} was doped, a blue shift of absorption edge is exhibited, attributed to the quantum size effect [20]. These demonstrate that La^{3+} dopant did not give rise to new spectrum phenomena, and could inhibit the growth of anatase crystallite. Moreover, it could also be seen that La^{3+} dopant improve the optic absorption performance of TiO_2 nanoparticles. Furthermore, the absorption of samples co-doped with Fe^{3+} and La^{3+} ion in the visible light rang is abruptly stronger than the undoped sample and doped sample with Fe^{3+} or La^{3+} alone.

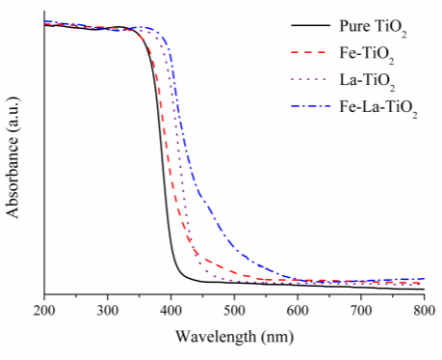

Fig. 4. UV–vis diffuse reflectance spectra of various samples.

3.6 Photocatalytic performance of the samples

Photocatalytic performance of the samples was evaluated by investigating the kinetics of the degradation reaction of MB in aqueous suspensions. Before irradiating suspensions, there is a slight loss of MB, the values are 6.7, 5.6, 8.1 and 9.3% of original MB concentration for pure TiO_2, Fe-TiO_2, La-TiO_2 and Fe-La-TiO_2 which were calcined at 500 ℃, due to adsorption of TiO_2 particles. However, most of the concentration decrease occurred during irradiation. Therefore, we conclude that the degradation of MB was due to chemical reaction rather than adsorption. For the comparison of reaction rate among different catalysts, the first-order kinetic model was introduced, $\ln C = -kt + \ln C_0$, where C is the MB concentration at time t, k is the apparent reaction rate constant and C_0 is the initial concentration. Under the experimental conditions used, we assume that concentration of MB after desorption–adsorption equilibrium is the initial concentration C_0. Fig. 5 shows the degradation of MB as a function of reaction time in the presence of different catalysts under visible-light irradiation. According to the above kinetic model, the rate constants k are found to be 0.0011, 0.0026, 0.0021, 0.0045 min^{-1} for pure TiO_2, Fe-TiO_2, La-TiO_2, Fe-La-TiO_2, respectively. Therefore, the visible-light reactivity of TiO_2 is significantly enhanced by these dopants, especially for Fe-La-TiO_2 catalyst. Fe-TiO_2 sample shows better photocatalytic activity than pure TiO_2. Science a new impurity levels were introduced between the conduction and valence band with the substitution for Ti^{4+} by Fe^{3+} in the structure of TiO_2, the electrons can be promoted from the valence band to these impurity levels [11]. This can induce more photo-generated electrons and holes to participate in the photocatalytic reactions. Therefore, Fe-TiO_2 has narrower band gap than pure TiO_2 and could increase the absorption in the visible-light region. Apart from this effect, Fe^{3+} ions can also serve as shallow trapping sites for charge carrier (e^- or h^+).

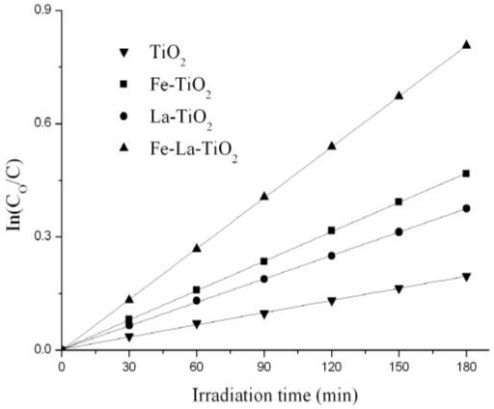

Fig. 5. The degradation of MB using different catalysts under visible-light irradiation.

The role of Fe^{3+} in the photocatalytic processes as shallow trapping sites was described [14]:

$$Fe^{3+} + e^- \rightarrow Fe^{2+} \quad (1)$$

$$Fe^{2+} + O_2 \rightarrow Fe^{3+} + O_2^- \quad (2)$$

$$Fe^{3+} + h^+ \rightarrow Fe^{4+} \quad (3)$$

$$Fe^{4+} + OH^- \rightarrow Fe^{3+} + \bullet OH \quad (4)$$

Since Fe^{3+} can act as electron and hole trap and they can separate the arrival time to the solution phase (Eqs.(2) and (4)) or the substrate, the recombination rate of the electron–hole pairs is lowered, therefore the photocatalytic activity is enhanced

La-TiO_2 also has better performance than pure TiO_2. On the one hand, La^{3+} dopant decrease the crystallite size (see Table 1) which facilitates the adsorption for MB; On the other hand, La^{3+} dopant could increase oxygen vacancies and/or surface defects in the TiO_2 photocatalysts

that might capture photoelectrons and inhibit the recombination between photoelectrons and holes, resulting in enhanced quantum efficiency [21].

Clearly, Fe-La-TiO_2 exhibits the highest photocatalytic activity for the degradation of MB. This may be owing to the synergistic effects of doped Fe^{3+} and La^{3+} on the enhancement of visible light activity as well as advantages of Fe^{3+} and La^{3+} singly doped. Fe^{3+} presents in the substitution positions in the TiO_2 lattice would introduce dopant energy levels into the band gap of TiO_2. Under visible light irradiation, the electrons can be promoted to these impurity levels, and then they were transferred to La^{3+} dopant within the crystal matrix or on the surface of TiO_2, which can enhance the electron–hole separation and the subsequent transfer of the trapped electrons to the adsorbed O_2 molecules. Thus, the photocatalytic activity efficiently improve.

Fig. 6 shows the degradation of MB using different catalysts under UV irradiation. According to the above first order kinetic model, the rate constants k are found to be 0.0148, 0.0122, 0.0164, 0.02 for pure TiO_2, Fe-TiO_2, La-TiO_2, Fe-La-TiO_2, respectively. It is shown that under UV light irradiation, the photocatalytic activity of Fe-TiO_2 decreased compared with pure TiO_2. Many electrons from the valence band were excited to the conduct band or these impurity levels introduced by Fe^{3+} dopant under UV irradiation owing to UV light with higher energy. However, these generated electrons would be trapped by Fe^{3+} in the lattice TiO_2 rather than be transferred to the surface. Meanwhile, many introduced holes could also be trapped by Fe^{3+}, thereby Fe^{3+} become the recombination center and result in the decrease of UV light photoactivity of Fe^{3+} doped TiO_2[34]. It can be ascribable to the detrimental effect of Fe^{3+} in increasing electron–hole recombination, which could explain by Eqs. (5) and (6):

$$Fe^{3+} + e^- \rightarrow Fe^{2+} \quad (5)$$

$$Fe^{2+} + h^+ \rightarrow Fe^{3+} \quad (6)$$

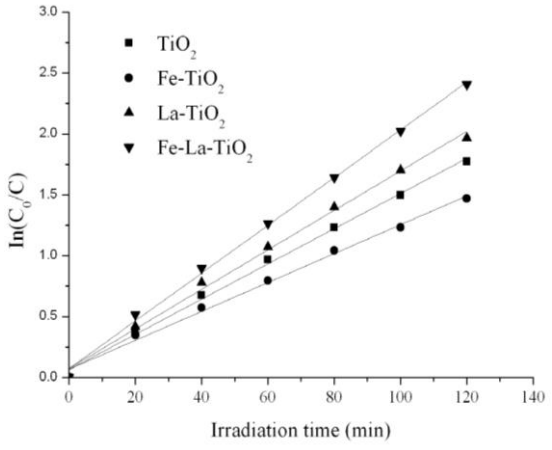

Fig. 6. The degradation of MB using different catalysts under UV irradiation.

Additionally, La-TiO_2 is more photoactive than TiO_2 because of the same positive role-played by La as under visible light irradiation. Compared to the other three samples, Fe-La-TiO_2 exhibits higher photocatalytic activity. The higher photoactivity of Fe-La-TiO_2 may be attributed to the following reasons. The synergistic effect of doped Fe^{3+} and La^{3+} is responsible for enhancement photocatalytic performance. Under UV light irradiation, the excited holes are trapped by Fe^{3+} dopant; meanwhile the remaining electrons can be trapped by La^{3+} and then transferred to the surface to initiate the photocatalytic processes. The mechanism of degradation of MB under UV light irradiation is different from that of under visible light. Under UV light irradiation, with respect to the Fe-La-TiO_2 sample, most of the electrons and holes are generated close to the surface and surface recombination is dominant process. When La^{3+} doped in the Fe-doped TiO_2, the excited electrons close to the surface are trapped by La^{3+} dopant, improving the charge separation and hence inhibition of surface recombination process.

4. Conclusions

Fe^{3+} and La^{3+} doped TiO_2 nanoparticles were synthesized. Results of various characterization methods indicate Fe^{3+} presents in the substitutional position in the lattice of TiO_2, and La^{3+} exists as La_2O_3 within the crystal matrix or on the surface of TiO_2. Photocatalytic experiments show that Fe^{3+} and La^{3+} have synergistically improved the photocatalytic activity of TiO_2 under both visible light and UV light irradiation. Explanations for the synergistic effect of Fe^{3+} and La^{3+} under visible light and UV light irradiation have been discussed. Under visible light irradiation, Fe^{3+} dopant plays a role in extending light absorption into the visible region and separating the arrival time to the surface, meanwhile La^{3+} dopant could restrain anatase-to-rutile phase transformation and inhibit the recombination between photoelectrons and holes. Under UV light irradiation, the excited holes are trapped by Fe^{3+}, meanwhile the remaining electrons are trapped by La^{3+} and then transferred to the surface to initiate the photocatalytic processes.

References

[1] R. Asahi, T. Morikawa, T. Ohwaki, K. Aoki, Y. Taga, Science., **293**, 269 (2001).
[2] Y. Yang, L. Qu, L. Dai, T. S. Kang, M. Durstock, Adv. Mater. **19**, 1239 (2007).
[3] A. Fujishima, T.N. Rao, D.A. Tryk, J. Photochem. Photobio. C.1 (2000) 1–21.
[4] K. Song, J. Zhou, J. Bao, Y. Feng, J. Am. Ceram. Soc. **91**, 1369 (2008).
[5] L. Cai, X. liao, B. Shi, Ind. Eng. Chem. Res. **49**, 3194 (2010).
[6] A. Ahmad, J. A .Shah, S. Buzby, S. I. Shah, Eur. J. Inorg. Chem., 948–953 (2008).
[7] S. In, A. Orlov, R. Berg, F. García,

S. Pedrosa-Jimenez, M. S. Tikhov, D. S. Wright, R. M. Lambert, J. Am. Chem. Soc. **129**, 13790 (2007).
[8] J. H. Jho, D. H. Kim, S. J. Kim, K. S. Lee, J. Alloys Compds. **459**, 386 (2008).
[9] Z. Liu, Y. Wang, W. Chua, Z. Li, C. Ge, J. Alloys Compds. **501**, 54 (2010).
[10] G. Colón, M. Maicu, M. C. Hidalgo, J. A. Navío, Appl. Catal. B: Environ. **67**, 41 (2006).
[11] X. Yang, C. Cao, L. Erickson, K. Hohn, R. Maghirang, K. Klabunde, J. Catal. **260**, 128 (2008).
[12] J. Zhu, J. Ren, Y. Huo, Z. Bian, H. Li, J. Phys. Chem. C, **111**, 18965 (2007).
[13] W. Choi, A. Termin, M. R. Hoffmann, J. Phys. Chem. **98**, 13669 (1994).
[14] Z. Ambrus, N. Balázs, T. Alapi, G. Wittmann, P. Sipos, A. Dombi, K. Mogyorósi. Appl. Catal. B: Environ **81**, 27 (2008).
[15] C. Wang, Q. Li, R. Wang, J. Mater. Sci. **39**, 1899 (2004).
[16] Y. Cong, J. Zhang, F. Chen, M. Anpo, D. He, J. Phys. Chem. C. **111**, 10618 (2007).
[17] A. Xu, Y. Gao, H. Liu, J. Catal. **207**, 151 (2002).
[18] M. Saif, M. S. A. Abdel-Mottaleb, Inorg. Chim. Acta **360**, 2863 (2007).
[19] C. Liu, X. Tang, C. Mo, Z. Qiang, J. Solid State Chem. **181**, 913 (2008).
[20] L. Jing, X. Sun, B. Xin, B. Wang, W. Cai, H. Fu, J. Solid. State. Chem. **177**, 3375 (2004).
[21] Y. Huo, J. Zhu, J. Li, G. Li, H. Li, J. Mol. Catal. A: Chem **278**, 237 (2007).
[22] I. Atribak, I. Such-Basanez, A. Bueno-Lopez, A. Garcia Garcia, Catal. Commun. **8**, 478 (2007).
[23] B. Tryba, J. Hazard. Mater. **151**, 623 (2008).
[24] X. Yang, C. Cao, L. Erickson, K. Hohn, R. Maghirang, K. Klabunde, J. Catal. **260**, 128 (2008).
[25] J. Choi, H. Park, M. Hoffmann, J. Phys. Chem. C. **114**, 783 (2010).
[26] S. C. Pillai, P. Periyat, R. George, D. E. McCormack, M. K. Seery, H. Hayden, J. Colreavy, D. Corr, S. J. Hinder, J. Phys. Chem. C **111**, 1605 (2007).
[27] Y. Zhang, S. G. Ebbinghaus, A. Weidenkaff, T. Kurz, H. K. Nidda, P. J. Klar, M. Güngerich. A. Reller, Chem. Mater. **15**, 4028 (2003).
[28] J. Zhu, F. Chen, J. Zhang, H. Chen, M. Anpo, J. Photochem. hotobiol. A. Chem. **180**, 196 (2006).
[29] X. Shen, J. Guo, Z. Liu, S. Xie, Appl. Surf. Sci. **254**, 4726 (2008).
[30] Yelda Yalç1n¸ M. Kılıç¸ Z. çınar, Appl. Catal. B: Environ. **99**, 469 (2010).
[31] J. Yu, Q. Xiang, M. Zhou, Appl. Catal. B: Environ. **90**, 595 (2009).
[32] A. M. D. Asha, J. T. S. Critchley, R. M. Nix, Surf. Sci. **405**, 201 (1998).
[33] A. M. Ruiz, A. Cornet, J. R. Morante, Sensor. Actuat. B **111**, 7 (2005).
[34] Y. Wu, J. Zhang, L. Xiao, F. Chen, Appl. Catal. B: Environ. **88**, 525 (2009).

*Corresponding author: shenfenglei@suda.edu.cn